

Measurements of plasma potential, radial electric field and turbulence rotation velocity in the T-10 tokamak

A.V. Melnikov¹, V.A. Vershkov¹, S.A. Grashin¹, L.G. Eliseev¹, S.E. Lysenko¹, V.A. Mavrin¹, S.V. Perfilov¹, D.A. Shelukhin¹, R.V. Shurygin¹, L.I. Krupnik², A.D. Komarov², A.S. Kozachok² and A.I. Zhezhera²

¹*Institute of Tokamak Physics, RRC "Kurchatov Institute", Moscow, Russia*

²*Institute of Plasma Physics, NSC KIPT, Kharkov, Ukraine*

Stabilization mechanisms by $E \times B$ shear likely play a role in the transition to better confinement plasma states: both edge and core transport barriers are related to an increase in the $E \times B$ sheared flow. The direct experimental study of plasma radial electric field E_r is the key issue to clarify $E \times B$ shear stabilization mechanisms. The plasma turbulence rotation velocity measurements, compared with $E_r \times B_t$ drift rotation velocity may explain, whether the turbulence moves together with the plasma or independently.

The absolute value of the core plasma potential φ was measured in the T-10 tokamak ($R = 1.5$ m, $a = 0.3$ m) by Heavy Ion Beam Probing (HIBP) diagnostic. The Ti^+ beam energy of HIBP was increased up to $E_b = 300$ keV, and the beam current up to 200 μA . This allows us to observe the core potential at high densities and in a wide radial area for the first time. At the limiter, the plasma potential and density were measured by Langmuir probes. The core plasma turbulence was studied by correlation reflectometry (CR).

The regimes with Ohmic (OH), on- and off-axis Electron Cyclotron Resonance (ECR) heating ($B_t = 1.55\text{--}2.4$ T, $I_p = 140\text{--}250$ kA, $\bar{n}_e = (1.3 - 4.1) \times 10^{19} \text{ m}^{-3}$, $P_{\text{EC}} < 1.5$ MW) were studied, see Table. In the regimes with $B_t = 1.55\text{--}2.08$ T, HIBP was able to extend the observation area from the plasma edge, $\rho = 1$, to the central region, $\rho = 0.25$ ($\Delta r = 6\text{--}30$ cm). The first regime, marked as I and II in Table (OH, $B_t = 1.55$ T, $I_p = 140$ kA,) is characterized by low line-averaged density, slowly evolving from $\bar{n}_e = 1.3$ to $2.4 \times 10^{19} \text{ m}^{-3}$ due to the gas puffing. The time traces of the main plasma parameters, including the potential $\varphi(0.21 \text{ m})$, are shown in Fig. 1(a). The plasma edge, $r = 0.25\text{--}0.3$ m, was probed with $E_b = 90$ keV. To extend the profile towards the centre, we increase E_b with the step of 10 keV up to 200 keV in a series of reproducible shots. The profiles, obtained in each shot, overlap with each other. The resulting radial profiles with length 23 cm are shown in Fig. 1(b). The profiles for three line-

averaged densities $\bar{n}_e = 1.3, 2.0$ and $2.4 \times 10^{19} \text{ m}^{-3}$ are marked with different colours. The plasma potential has the negative sign in the whole observed area. The $\varphi(r)$ profile presents linear-like function with the lowest absolute value at the deepest point $\varphi(0.07 \text{ m}) = -1.5 \text{ kV}$. The slope of the profile allows us to estimate the mean radial electric field E_r : for the lowest density $E_r \sim -5.5 \text{ kV/m}$. Figure 1(b) shows that the potential well becomes deeper, and E_r becomes more negative up to $E_r \sim -6.5 \text{ kV/m}$ with the rise of density and energy confinement time τ_E . This result is consistent with earlier measurements in TM-4 [1] and TJ-II [2].

The regime III, ($B = 2.08 \text{ T}$, $\bar{n}_e = 2.4 \times 10^{19} \text{ m}^{-3}$, $I_p = 165 \text{ kA}$, $P_{EC} = 0.9 \text{ MW}$) with off-axis ECRH ($\rho_{ECRH} = 0.5$) has the current ramp-up to $I_p = 212 \text{ kA}$ at the ECRH phase. The time traces of the main plasma parameters are shown in Fig. 2. The potential profile evolution is shown in Fig. 3. In OH phase, $\varphi(r)$ presents linear-like function with the lowest absolute value at the deepest point $\varphi(0.07 \text{ m}) = -1.6 \text{ kV}$, and correspondingly the mean E_r is -7.0 kV/m . In the ECRH phase, the absolute potential well becomes significantly shallower, $\varphi(0.07) = -1.3 \text{ kV}$, and E_r decreases to $\sim -5.5 \text{ kV/m}$. After current ramp-up, $\varphi(r)$ slightly decreases, and E_r decreases up to $\sim -4.7 \text{ kV/m}$. The estimated error $\Delta E_r = \pm 0.3 \text{ kV/m}$ for this regime. Note that during the ECRH phase the plasma potential profile keeps its linear-like shape. No strong irregularity has been observed on the $\varphi(r)$ profile at the area of ECRH power deposition. At the inner radii respect to the power deposition, $\varphi(r)$ still keeps its linear-like shape. After the ECRH switch-off, in the OH regime with $I_p = 212 \text{ kA}$, $\varphi(r)$ returns to its initial shape, corresponding to the OH regime with $I_p = 165 \text{ kA}$. These observation shows that the potential is not a strong function of I_p .

The high B_t OH regime IV ($B_t = 2.4 \text{ T}$, $\bar{n}_e = 4.1 \times 10^{19} \text{ m}^{-3}$, $I_p = 200 \text{ kA}$) allows HIBP to observe the outer half of the plasma column ($\Delta r = 16-27 \text{ cm}$) only with highest possible $E_b = 300 \text{ keV}$. Similar to the previous cases, $\varphi(r)$ presents linear-like function, as shown in Fig. 4, with the lowest absolute value at the deepest point $\varphi(0.16 \text{ m}) = -1.2 \text{ kV}$, mean $E_r \sim -9.0 \text{ kV/m}$ $\pm 0.5 \text{ kV/m}$.

At all observed regimes, $E_r(r) \sim \text{const}$ in the radial range of HIBP measurements. The plasma column rotates not as a rigid body due to the $B_t(r)$ dependence. The typical values for $E \times B$ drift velocity are $V_{E \times B} \sim 3.0 \text{ km/s}$, $\Omega_{E \times B} \sim 1.5 \times 10^4 \text{ radian/s}$ for the Ohmic stage, and $V_{E \times B} \sim 2.4 \text{ km/s}$, $\Omega_{E \times B} \sim 1.25 \times 10^4 \text{ radian/s}$ for the ECRH stage.

The broadband turbulence rotation velocity Ω_{TURB} was measured by CR in the regime III at the same discharges as HIBP, but in different poloidal position. To compare with Ω_{TURB} , we take $\Omega_{E \times B} = E_r/rB_t$ with E_r obtained by HIBP and B_t along the x coordinate of CR

measurements. The experimental layout is shown in Fig. 5. CR antennae are located at 90° anticlockwise from HIBP along the torus. Figure 6 (a,B) shows that $\Omega_{\text{TURB}}(r)$ is close to $\Omega_{E \times B}(r)$ in the whole observed radial range both in OH and ECRH plasmas. It is important to note that during the ECRH phase, $\Omega_{\text{TURB}}(r)$ does not show any strong irregularity in the area of ECRH power deposition, similar to $\Omega_{E \times B}(r)$.

Finally, the mean $\varphi(r)$ exhibits the linear-like shape suggesting $E_r \sim \text{const}$. Negative $\varphi(r)$ in the deepest point (smallest radii) and E_r both tends to be higher for higher densities and lower with ECRH, i.e. a stronger negative E_r is associated to better energy confinement time τ_E . Within the achieved experimental accuracy, the broadband drift-wave turbulence tends to rotate with the plasma $E \times B$ rotation velocity.

This work is supported by Grants: FASI 02.740.11.5062, RFBR 08-02-01326, 10-02-01385.

References

- [1] V.I. Bugarya et al., Nucl. Fusion 25, 1701 (1985).
- [2] A.V. Melnikov et al., Fusion Sci. Techn. 31, 51 (2007).

Table 1. Parameters of studied regimes.

Regime	\bar{n} , 10^{19} m^{-3}	E_r , V/cm	Δr , cm	B_t , T	I_p , kA	τ_E , ms
I	1.3	55	6-30	1.55	140	20
II	2.4	65	6-30	1.55	140	36
III	2.5	70	7-22	2.08	165	52
IV	4.1	90	16-27	2.4	210	58

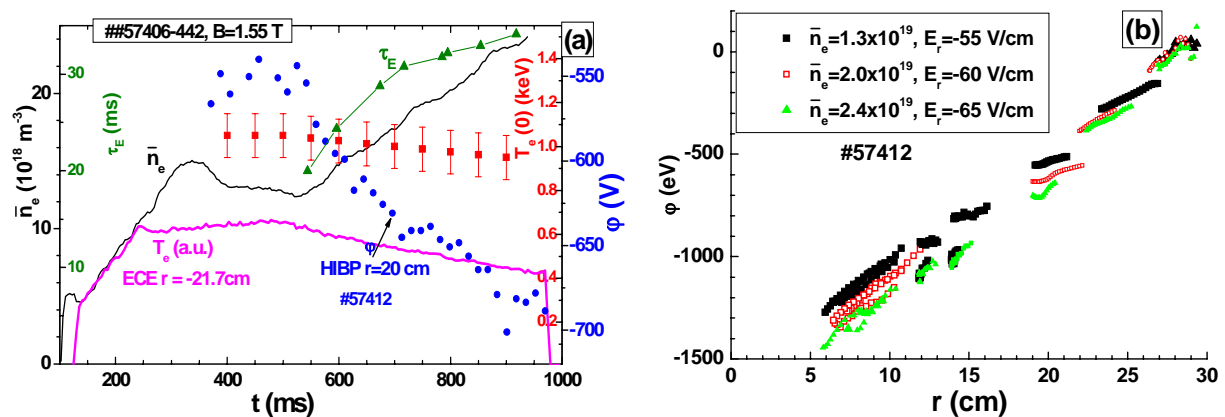


Fig. 1. (a) Evolution of density n_e , potential φ , energy confinement time τ_E and electron temperature $T_e(0)$ (red ■) by SXR-spectrograph in the regime I, II with density ramp-up. (b) The potential profile combined from the set of the scans for three densities $\bar{n}_e = 1.3 \times 10^{19} \text{ m}^{-3}$ (black ■), 1.8 (red □) $2.4 \times 10^{19} \text{ m}^{-3}$ (green ▲).

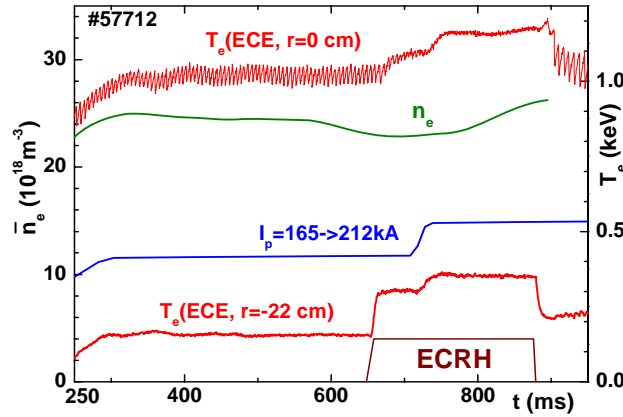


Fig. 2. Evolution of density and temperature in regime III with ECRH and current ramp-up.

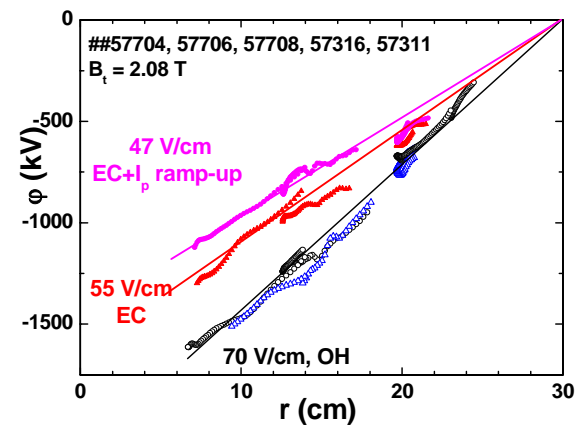


Fig. 3. Potential profiles in regimes III with ECRH and current ramp-up.

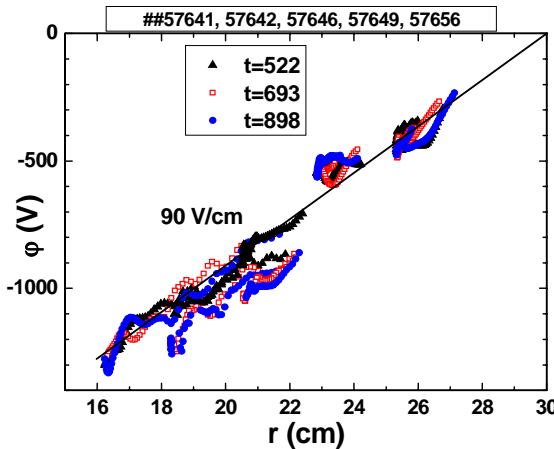


Fig. 4. The potential profiles in OH high-density regime IV.

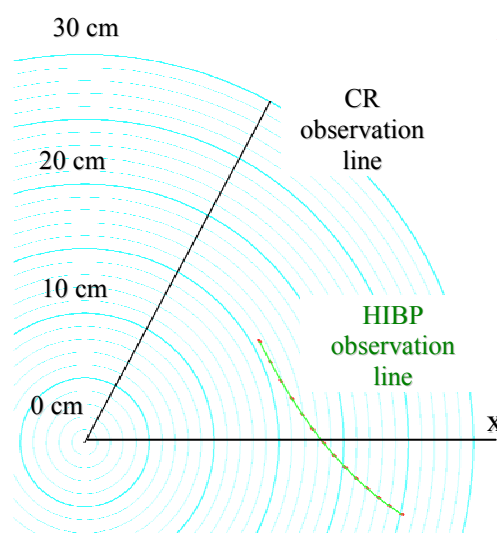
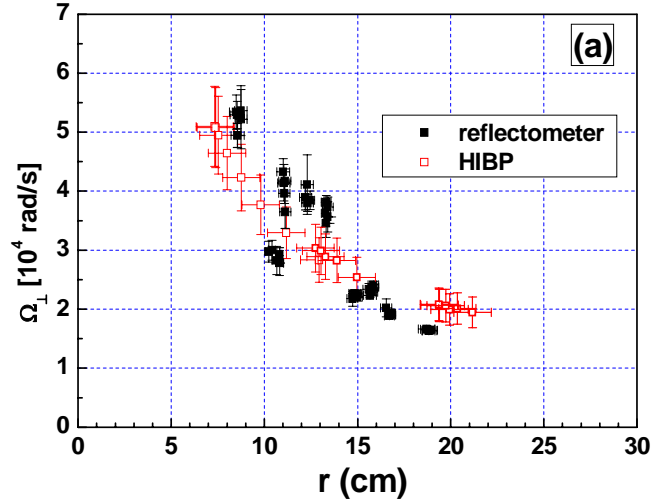


Fig. 5. Experimental layout for comparative HIBP and CR rotation measurements.

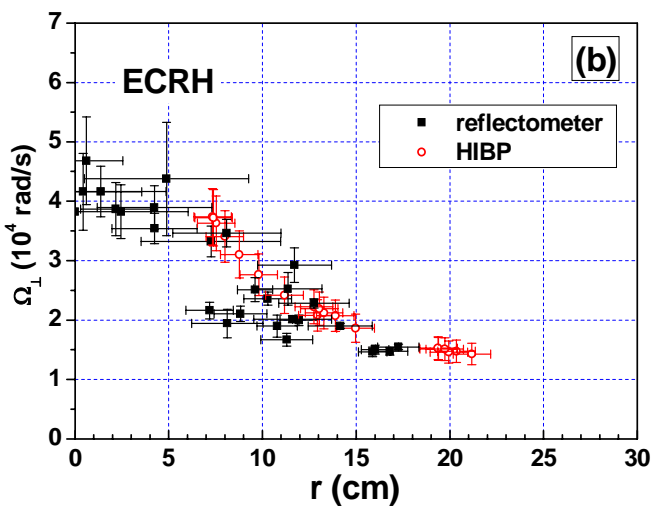


Fig. 6. Comparison of rotation velocities of density perturbations Ω_{TURB} from CR, with core plasma rotation Ω_{ExB} from HIBP in OH (a) and ECRH (b) plasmas.